Earth Systems and Environment (2019) 3:429–444
https://doi.org/10.1007/s41748-019-00133-w

REVIEW ARTICLE

Identification of Potential Drought Areas in West Africa Under Climate Change and Variability

Gandome Mayeul L. D. Quenum[1,2] · Nana A. B. Klutse[3] · Diarra Dieng[4] · Patrick Laux[4] · Joël Arnault[4] · Japhet. D. Kodja[2] · Philip G. Oguntunde[5]

Received: 15 September 2019 / Accepted: 14 October 2019 / Published online: 30 October 2019

Abstract

The study investigates how the rising global temperature will affect the spatial pattern of rainfall and consequently drought in West Africa. The precipitation and potential evapotranspiration variables that are obtained from the Rossby Centre regional atmospheric model (RCA4) and driven by ten (10) global climate models under the RCP8.5 scenario were used. The model data were obtained from the Coordinated Regional Climate Downscaling Experiment (CORDEX) and analyzed at four specific global warming levels (GWLs) (i.e., 1.5 °C, 2.0 °C, 2.5 °C, and 3.0 °C) above the pre-industrial level. This study utilized four (4) indices: the standardized precipitation index, the precipitation concentration index, the precipitation concentration degree, and the precipitation concentration period over West Africa to explore the spatiotemporal variations in the characteristics of precipitation concentrations. Additionally, studying the impact of the four GWLs on consecutive dry days, consecutive wet days, and frequency of the intense rainfall events led to a better understanding of the spatiotemporal pattern of extreme precipitation. The results show that, at each GWL studied, the onset of rainfall comes 1 month earlier in the Gulf of Guinea compared to the historical period (1971–2000) with increasing rainfall intensity in the whole study domain, and the northeastern part of the study area becomes wetter. The rainfall concentration is uniformly distributed over the Gulf of Guinea and the Savanna zone for both the historical period and RCP8.5 scenario, while the Sahel zone which has shown an irregular concentration of rainfall for the historical period shows a uniform concentration of rainfall under all four GWLs.

Keywords Extreme drought events · Specific global warming levels · CORDEX · West Africa · Precipitation concentration

1 Introduction

Precipitation variability under global warming is strongly connected to extreme events, which pose threats to the environment and society (IPCC 2012), and can also have devastating consequences on ecosystems, food supply, and economies (Easterling et al. 2000). Droughts and floods are direct extreme events attributed to precipitation variability which involve detrimental consequences in West Africa (Ebi and Bowen 2016). The drought that affected West African countries from the beginning of the 1970s lasted for several decades and is one of "the most undisputed and largest recent climate changes recognized by the climate research community" (Dai et al. 2004). Literature provides a good review of droughts in association with rainfall variability over West Africa (Le Barbé et al. 2002; Lebel and Ali 2009; Paturel et al. 1998).

The increases in surface air temperatures lead to a higher water vapor amount in the atmosphere and the change in

✉ Nana A. B. Klutse
nklutse@ug.edu.gh

Gandome Mayeul L. D. Quenum
malgdaq2000@yahoo.fr

1 West African Science Service Centre for Climate Change and Adapted Land Use (WASCAL), Graduate Research Program in West African Climate System (GRP-WACS), Federal University of Technology, Akure (FUTA), Akure, Nigeria

2 National Institute of Water (NIW), 01 BP 4521, Cotonou, Bénin

3 Department of Physics, University of Ghana, Legon, Accra, Ghana

4 Kalrsruhe Institute of Technology, Campus Alpin, Institute of Meteorology and Climate Research (IMK-IFU), Kreuzeckbahnstrasse 19, 82467 Garmisch-Partenkirchen, Germany

5 Department of Agricultural and Environmental Engineering, Federal University of Technology, Akure, Nigeria

spatiotemporal precipitation patterns which contribute to the large precipitation differences in different regions of the world (Chou and Lan 2011; Gao et al. 2014). Kasei et al. (2010) evaluated the temporal characteristics of meteorological droughts by analyzing the intensity, the areal extent and the recurrence frequency in the Volta basin, a semiarid region in West Africa. The study reported 5 years (1961, 1970, 1983, 1992, and 2001) within the study period 1961–2005 where 75% of West Africa was under historical droughts. Many authors (Fiala et al. 2010; Petrow and Merz 2009; Sung and Chung 2014; and Van De Giesen et al. 2010) used an indicator based on the threshold to characterize drought and flood events. For instance, meteorological indices such as the standardized precipitation index (SPI, e.g., Joetzjer et al. 2013; Vicente-Serrano et al. 2012; Zargar et al. 2011; and Zhai et al. 2010) and Palmer Drought Severity Index (PDSI) (Palmer 1965; Abatzoglou et al. 2014) are commonly used to quantify hydrological drought. These meteorological approaches were also used by Garner et al. (2015), Teuling et al. (2013), and Trambauer et al. (2014) to find numerous thresholds, which allow the identification of extreme river flow events. A recent agreement on the increase in rainfall since the beginning of the 2000s is identified by L'Hôte et al. (2002), Lebel and Ali (2009) and Lebel et al. (2009). Hence, Descroix et al. (2012) and Panthou et al. (2014) showed an intensification of the rainfall regime in the Sahelian region since the 2000s, characterized by a greater contribution of extreme precipitation to the annual total rainfall.

The precipitation concentration indices play an important role in the total annual precipitation amount, the extent, and the intensity of extreme precipitation events. These indices have the potential to quantify/or to monitor floods and droughts events, which are expected to put considerable pressure on water resources (Zhang and Qian 2003; and Zhang et al. 2009). Precipitation concentration indices have been used in several studies including the precipitation concentration index (PCI) elaborated by Oliver (1980), modified by De Luis et al. (2011), and used by Shi et al. (2015) as an indicator of rainfall concentration for annual and seasonal scales. Ezenwaji et al. (2017) applied the PCI to investigate the implication of the concentration and variability of rainfall on flooding over Awka Urban Area (Nigeria). Furthermore, the precipitation concentration degree (PCD) and the precipitation concentration period (PCP) were redefined by Zhang and Qian (2003) in a study of droughts and floods over China. The basic concept behind the PCD and PCP is that the monthly total precipitation is a vector quantity with both magnitude and direction (Li et al. 2011; Wang et al. 2013).

Extreme rainfall is projected to increase in frequency and intensity over Africa (IPCC 2014, SR1.5). Abiodun et al. (2018), Egbebiyi (2016), Klutse et al. (2018), Kumi and Abiodun (2018), Maúre et al. (2018), and Nikulin et al. (2018) assessed extreme climate indices under different GWLs for different climate zones in Africa. The methodologies and the variables employed in these studies are vital for effective adaptation and mitigation strategies. Therefore, this study aims to use one type of drought indicator, SPEI to classify the present and future drought areas in West Africa, which is strongly influenced by the spatial distribution of rainfall. The indices PCI, PCD, PCP are therefore used to explain the spatial and temporal variability of precipitation. Among the precipitation indices, the consecutive dry day (CDD) and consecutive wet day (CWD) are used in this study to explain the maximum dry days and maximum wet days of global warming level 1.5 °C, 2.0 °C, 2.5 °C, 3.0 °C.

2 Description of the Study Areas and Methodology

2.1 Study Area and Data

The investigation area, West Africa covers the domain located between latitudes 0°N and 20°N and longitude 20°W and 20°E (Fig. 1). This region is bordered in the south by the Gulf of Guinea, in the north by Mauritania, Mali, and Niger, while the Cameroon Highlands and the Atlantic Ocean form, respectively, the eastern boundary and the western limit. The annual mean temperature is about 18 °C but in the Sahel, maximum temperatures can reach above 40 °C. Ocean currents and local features such as topography mostly affect rainfall patterns over this region. In terms of climatic zones, West Africa can be divided into three different regions. The first region covers the Sahel and is characterized as a semiarid zone located from western Senegal to eastern Sudan between 12°N and 20°N. The second zone is the Sudano-Sahelian and the third zone comprises the Guinea coast, which is characterized by a two rainy season driven by the Inter-Tropical Discontinuity (ITD).

The evaluations of the four droughts indicators are done by using the precipitation and the potential evapotranspiration datasets from CORDEX (Nikulin et al. 2012) and driven by RCA4 at daily and monthly timesteps. The simulated dataset at $0.44° \times 0.44°$ resolution covers the period form 1971 to 2100. And the evaluation period is from 1971 to 2000 as the historical period and from 2006 to 2100 for the future projections. The GWLs reference values of the study are pre-industrial scenarios and RCP8.5: 1.5 °C, 2.0 °C, 2.5 °C, and 3.0 °C. Table 1 inspired from Déqué et al. (2017) summarizes the classifications of the 30-year projection of each GWL. The gridded climate research unit (CRU v3.23, monthly at 0.5° horizontal resolution, 1901–2014; Harris et al. 2014) provided by the University of East Anglia and prepared based on the archive of monthly mean precipitation

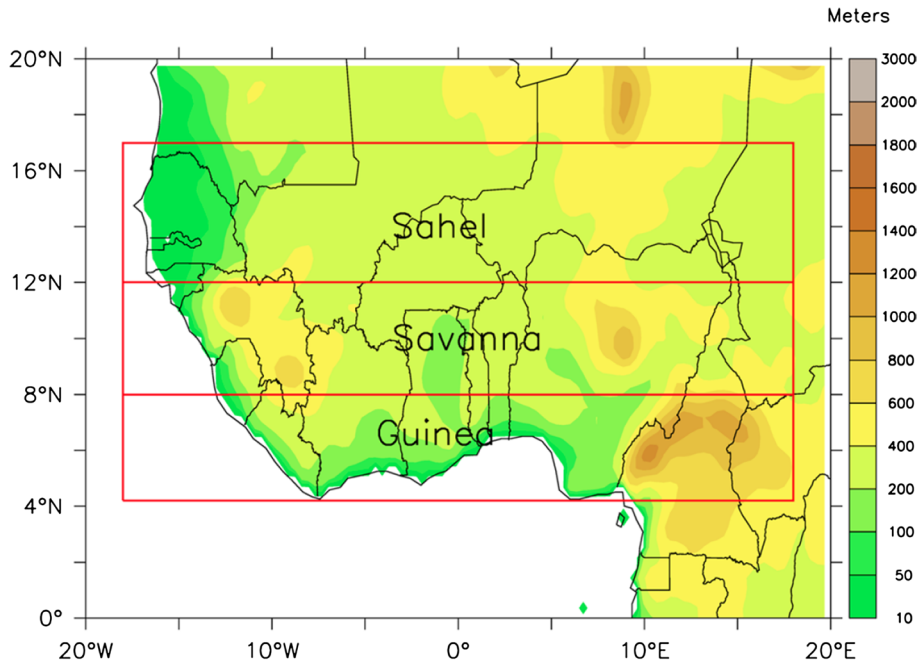

Fig. 1 Study domain showing West African topography and the area of focus: Gulf of Guinea (Guinea), Savanna, and Sahel

Table 1 Recapitulative of selected years of RCA4 models according to each global warming level (Déqué et al. 2017)

RCM	RCP8.5				
	GCM	1.5 °C	2.0 °C	2.5 °C	3.0 °C
RCA4	CanESM2	1999–2028	2012–2041	2024–2053	2034–2063
	CNRM-CM5	2015–2044	2029–2058	2041–2070	2052–2081
	CSIRO-Mk3	2018–2047	2030–2059	2040–2069	2050–2079
	EC-EARTH-r12	2005–2034	2021–2050	2034–2063	2047–2076
	GFDL-ESM2 M	2020–2049	2037–2066	2052–2081	2066–2095
	HadGEM2-ES	2010–2039	2023–2052	2033–2062	2042–2071
	IPSL-CM5A-MR	2002–2031	2016–2045	2027–2056	2036–2065
	MIROC5	2019–2048	2034–2063	2047–2076	2058–2087
	MPI-ESM-LR	2004–2033	2021–2050	2034–2063	2059–2088
	NorESM1-M	2019–2048	2034–2063	2047–2076	2059–2088

and temperature provided by more than 4000 weather stations distributed all over the world.

2.2 Methodology

2.2.1 Standardized Precipitation Evapotranspiration Index (SPEI)

SPEI is an index computed based on the non-exceedance probability of the climate water balance described by Eq. (1), which relies on the differences between the precipitation (PRE) and the potential evapotranspiration (PET), adjusted using a three-parameter log-logistic distribution which accounts for common negative values (Vicente-Serrano et al. 2010). The SPEI uses a three-parameter distribution to capture the deficit values since it is most likely that in arid and semiarid areas the moisture deficit can be negative. For two-parameter distributions as used in case of SPI, the variable x has a lower boundary of zero ($0 > x < \infty$) meaning that x can only take positive values while for the three-parameter distributions used in SPEI, x can take values in the range ($\gamma > x < \infty$) implying that x can also take negative values; γ is the parameter of origin of the distribution (Vicente-Serrano et al. 2010). The SPEI is obtained by normalizing the water balance into the log-logistic probability distribution. Assume D_n as the difference between PRE and PET for the month n.

$$D_n = \mathrm{PRE}_n - \mathrm{PET}_n \quad (1)$$

The calculated D values are aggregated at different timescales as follows:

$$D_n^k = \sum_{i=0}^{k-1} \mathrm{PRE}_{n-1} - \mathrm{PET}_{n-1} \tag{2}$$

where k is the timescale (months) of the aggregation and n is the particular month for which the climate water balance is computed.

The probability density function of a log-logistic distribution is given as:

$$f(x) = \frac{\beta}{\alpha}\left(\frac{x-\gamma}{\alpha}\right)^{\beta-1}\left(1+\left(\frac{x-\gamma}{\alpha}\right)^{\beta}\right)^{-2} \tag{3}$$

where α, β and γ are, respectively, scale, shape, and origin parameters for $\gamma > D < \infty$. The probability distribution function for the D series is then given as:

$$f(x) = \left[1+\left(\frac{\alpha}{x}-\gamma\right)^{\beta}\right]^{-1} \tag{4}$$

With $f(x)$, the SPEI can be obtained as the standardized values of $F(x)$ according to the method of Abramowitz and Stegun (1964):

where

$$\mathrm{SPEI} = W - \frac{C_0 + C_1 W + C_2 W^2}{1 + d_1 W + d_2 W^2 + d_3 W^3} \tag{5}$$

and

$$W = -2\ln(P) \tag{6}$$

for $P \leq 0.5$, P is the probability of exceeding a determined D value, P=1−$F(x)$.

If $P > 0.5$, P is replaced by $1-P$ and the sign of the resultant SPEI is reversed. The constants are: $C_0 = 2.515517$, $C_1 = 0.802853$, $C_2 = 0.010328$, $d_1 = 1.432788$, $d_2 = 0.189269$, $d_3 = 0.001308$

The computation of the SPEI is done over each grid point for each dataset. The SPEIs have been calculated for 1 month, 3 months, 6 months and 12 months. Table 2 presents its classification according to the moisture state.

Table 2 Classification of moisture level with the SPEI

SPEI value	Moisture level
+ 2.0 and greater	Extremely wet
+ 1.5 to 1.99	Very wet
+ 1 to 1.49	Moderately wet
− 0.99 to 0.99	Near normal
− 1.49 to − 1.0	Moderately dry
− 1.99 to − 1.5	Severely dry
Less to − 2.0	Extremely dry

2.2.2 Calculation of Precipitation Concentration Index (PCI)

PCI elaborated by Oliver (1980) and modified by De Luis et al. (2011), and also used by Shi et al. (2015) was employed as an indicator of rainfall concentration for annual and seasonal scales (wet and dry seasons). The precipitation concentration index (PCI) was then tested to find out the eventual trend of rainfall spatial distribution. As per Oliver (1980), a uniform precipitation distribution (i.e., low precipitation concentration) refers to PCI values less than 10, when PCI values are between 11 and 15 indicating a moderate precipitation concentration and, for PCI values between 16 to 20, representing an irregular distribution; finally, values above 20 represent a strong irregularity (i.e., high precipitation concentration) in the precipitation distribution (Table 3). The following equations were used on each grid point to calculate the PCI.

$$\mathrm{PCI}_{\mathrm{annual}} = \frac{\sum_{i=1}^{12} P_i^2}{(\sum_{i=1}^{12} P_i)^2} \times 100 \tag{7}$$

$$\mathrm{PCI}_{\mathrm{wet}} = \frac{\sum_{i=1}^{\mathrm{nw}} P_i^2}{(\sum_{i=1}^{\mathrm{nw}} P_i)^2} \times \frac{100 * \mathrm{nw}}{12} \tag{8}$$

$$\mathrm{PCI}_{\mathrm{dry}} = \frac{\sum_{i=1}^{\mathrm{nd}} P_i^2}{(\sum_{i=1}^{\mathrm{nd}} P_i)^2} \times \frac{100 * \mathrm{nd}}{12} \tag{9}$$

Equation (7) is used for annual PCI, while Eqs. (8) and (9) are utilized for seasonal scales (respectively, rainy, and dry seasons). nw and nd represent, respectively, the number of rainy and dry season months; p = precipitation of ith month. To investigate the change in PCI, 30 years were considered for both historical (1971–2000) and future periods (2006–2100). Table 1 shows the projection periods used for each GWL.

2.2.3 Computation of Precipitation Concentration Degree (PCD) and Precipitation Concentration Period (PCP)

The PCD and PCP were proposed by Zhang and Qian (2003) to measure the rainfall distribution and the peak rainfall date.

Table 3 Classification of PCI

PCI value	Precipitation distribution state
10 ≤ PCI	Uniform precipitation distribution
11 ≤ PCI ≤ 15	Moderate precipitation distribution
16 ≤ PCI ≤ 20	Irregular precipitation distribution
PCI ≥ 20	Strong irregular precipitation distribution

The concept is based on the daily or monthly total precipitation. It can be assumed that total precipitation on a timescale (daily, 5 days, weekly, decade, or monthly) is a vector quantity and that the direction for a year can be seen as a circle (360°). According to Li et al. (2011) and Zhang and Qian (2003), the indices were calculated as follows:

$$\theta_j = \left(360^\circ * \frac{j}{n}\right) \tag{10}$$

$$R_i = \sum r_{ij} \tag{11}$$

$$R_{xi} = \sum_{j=1}^{N} r_{ij} * \sin\theta_j \tag{12}$$

$$R_{yi} = \sum_{j=1}^{N} r_{ij} * \cos\theta_j \tag{13}$$

$$\mathrm{PCD}_i = \frac{\sqrt{R_{xi}^2 + R_{yi}^2}}{R_i} \tag{14}$$

where i is the year (e.g., for pre-industrial period $i = 1971, 1972, \ldots, 2000$), j represents the timescale (daily, 5 days, weekly, decade, or monthly) of that year, R_i is the amount of rainfall of a year, r_{ij} is the precipitation of the jth timescale in the ith year, n is the number of timescale per a year (e.g., daily: for a non-leap year, $n = 365$, while in a leap year, $n = 366$)

$$\alpha_i = \tan^{-1}\left(\frac{R_{xi}}{R_{yi}}\right) \tag{15}$$

$$D_i = \begin{cases} \alpha_i \ \left(R_{yi} > 0, R_{xi} \geq 0\right) \\ \alpha_i \ \left(R_{yi} > 0, R_{xi} < 0\right) \\ \alpha_i \ \left(R_{xi} < 0\right) \end{cases} \tag{16}$$

$$\mathrm{PCP}_i = D_i * \left(\frac{n}{360^\circ}\right) \tag{17}$$

3 Results and Discussion

3.1 Evaluation of the Climate Variables

The ensemble mean of models (referred as RCMEAN) appropriately represents, over West Africa, moisture variables such as precipitation (PRE), the potential evapotranspiration (PET), and the climate water balance (CWB = PRE-PET) with a very good and significant (99% of confidence level) correlation ($r \geq 0.90$) compared to observed CRU. The precipitation is well reproduced regarding the observed CRU. The model was able to capture the spatial gradient of precipitation over the study area, with well-located maxima (maximum around the Gulf of Guinea and minimum in the Sahel), with some scattering location of the maximum rainfall in southern of Nigeria, Guinea-Conakry, and Liberia, and the west of Cameroun. In terms of amount, the bias pattern shows that RCMEAN globally fairly overestimates the precipitation except the southeastern part of the study domain where the model displays an underestimation of the precipitation. From the assessment of the climate water balance (Fig. 2g–i), it can be seen a very important water deficit (negative bias) in the Savanna and Gulf of Guinea, which is due to the underestimation of precipitation, while in the Sahel, there is a surplus of water. However, particularly high values are recorded around coastal countries as Liberia, Sierra Leone, and southern Nigeria.

The inconsistency of the climate water balance assessment between the simulated models and observed can be assigned to various factors. For instance, the wet (positive values) bias over western part of the study area indicates that the convective parameterization schemes at 0.44° horizontal resolution in RCA4 model may be too active in producing precipitation over this area (Abiodun et al. 2018), while the dry (negative values) bias over the eastern part of the study area suggests that the convective parameterization schemes are not fully resolved over the eastern area, producing less moisture available for inland rainfall. It can also be due to the density of the weather stations available over the area (both Eastern and Western) for the observed data estimation. The method of calculating PET can also be a factor of the disparity. Abiodun et al. (2018) assessed the uncertainty of PET estimation with Hargreaves and Penman methods and found that its uncertainty contributes to the CWB's divergence.

The annual cycle of precipitation presented in Fig. 3 lies within the model ensemble spread in all the sub-zones, and the ensemble mean closely follows the observed curve. In the Gulf of Guinea, RCMEAN and CRU indicate two rainy seasons, while the Savannah and Sahel have shown a single-mode diet with a dry season (dry winter) and a single rainy season (wet summer). These observations reflect the seasonal fluctuations (oscillation) of the ITD over West Africa. The average value of precipitation over the Gulf of Guinea and Savanna is increasing from the second part of May up to a peak (180 mm month^{-1} for the Gulf of Guinea and 230 mm month^{-1} for the Savanna) in August when the ITCZ reached its most northerly position (second quasi-stable position) about 10°N. The average rainfall value in

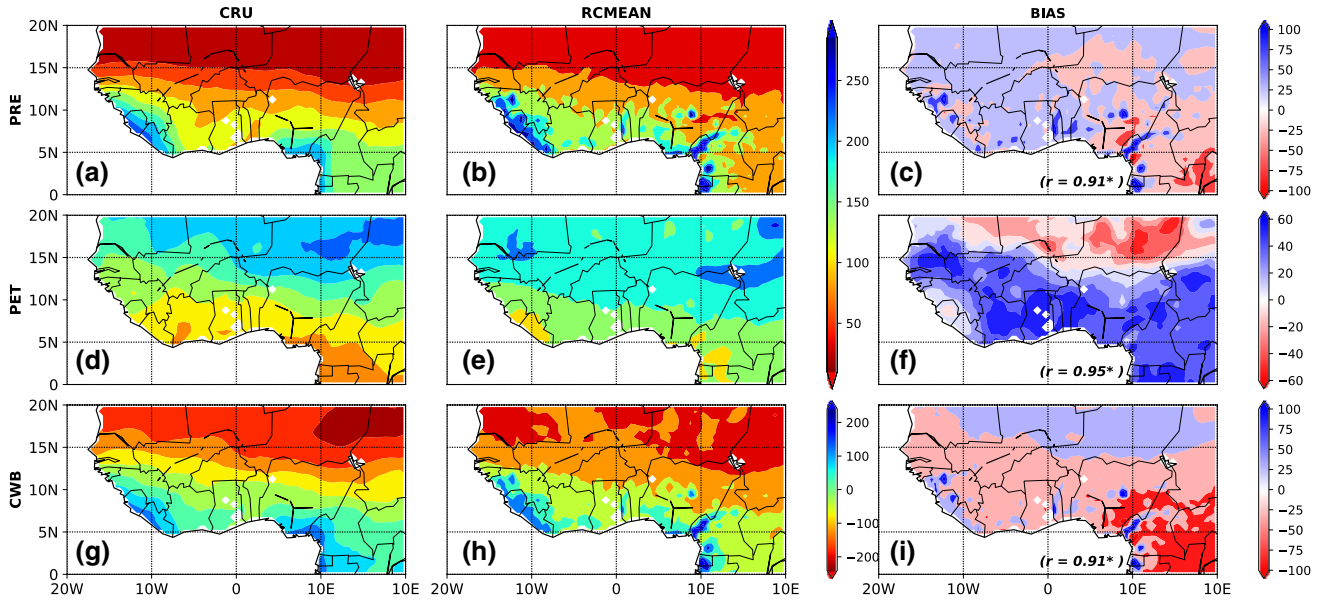

Fig. 2 Spatial distribution of climate variables for CORDEX RCA4 models ensemble (RCMEAN) and CRU over West Africa for the historical period (1971–2000). The climate variables are: precipitation (PRE, mm month^{-1}), the potential evapotranspiration (PET, mm month^{-1}), and the climate water balance (CWB = PRE-PET, mm month^{-1}). r is the correlation between the observed CRU and RCMEAN, and the bias is the difference between them (bias: RCMEAN-CRU). The asterisks (*) explain the correlation which is statistically significant at 99% of confidence level

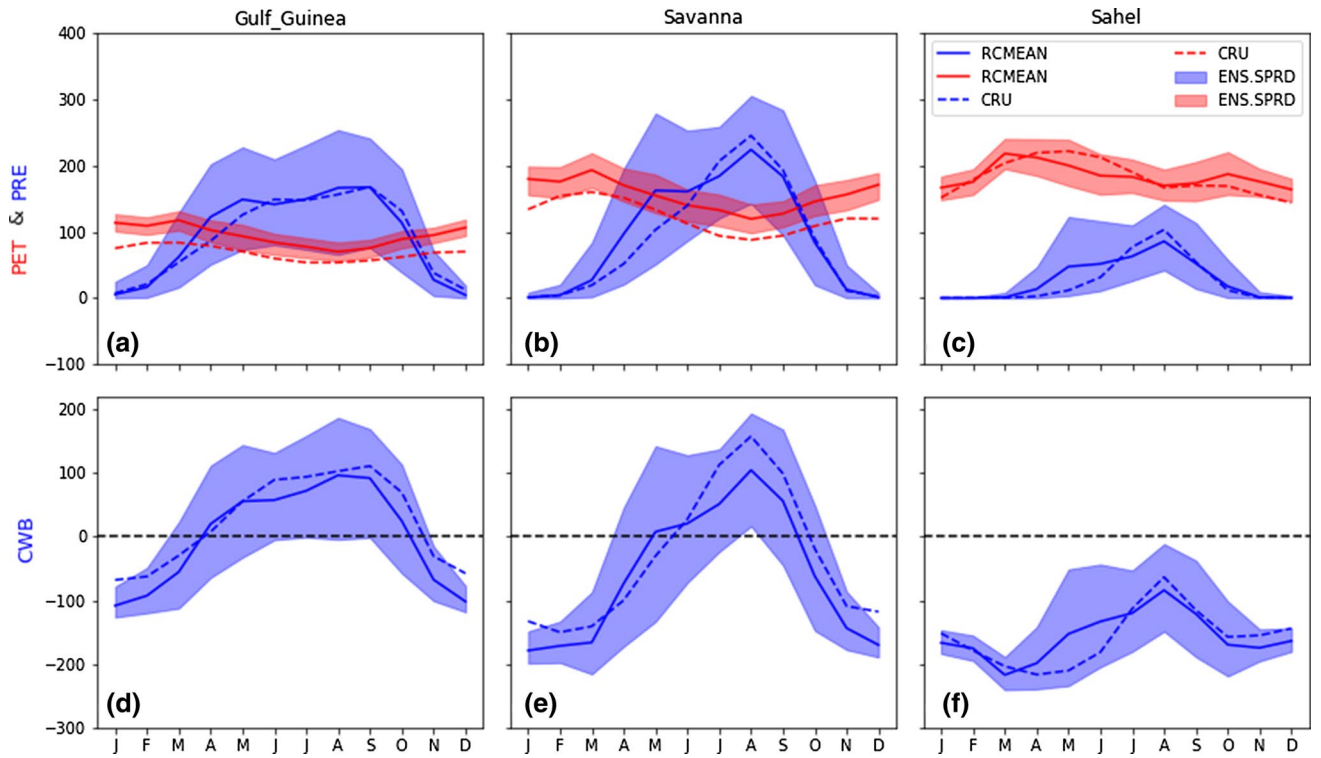

Fig. 3 Annual cycle of the climate variables (precipitation (PRE : mm month^{-1}), potential evapotranspiration (PET : mm month^{-1}), and the climate water balance (CWB = PRE-PET, mm month^{-1})) over the three main zones of the study area (Gulf of Guinea, Savanna and Sahel). RCMEAN represents the ensemble mean (solid line) of simulated model, and ENS.SPRD is the spread of CORDEX-RCA4 simulations. The dashed line presents the CRU variable

the Sahel also peaked in August, but showed a later increase (July) compared to other regions. The driest period is from October to March in the Gulf of Guinea and from October to May for the Savanna, where the PET increases till reaching its maximum value. It can also be noticed that during the rainy season the PET value dropped to its minimum value. The observed value does not lie within the model spread but follows the model's curve and underestimates the simulations over the Gulf of Guinea and Savanna. The Sahel is dry for the whole year because the CWB is negative for the historical period. The PET here agreed well by lying within the models and follows the curve of simulations.

According to the good agreement of the models with respect to the observed (Figs. 2, 3), the evaluation of the spatial pattern to detect potential drought and flooding areas is performed using the SPEI for various scales to focus on different types of droughts. The SPEI1 is used to characterize the meteorological drought, while the couple (SPEI3, SPEI6) and (SPEI9, SPEI12) are referred to agricultural and hydrological droughts, respectively. Figure 4 shows that RCMEAN reproduces the patterns in phase opposition (with negative correlation). This opposite performance may be due to various factors. It can be related to the temporal gridded average for each model and the

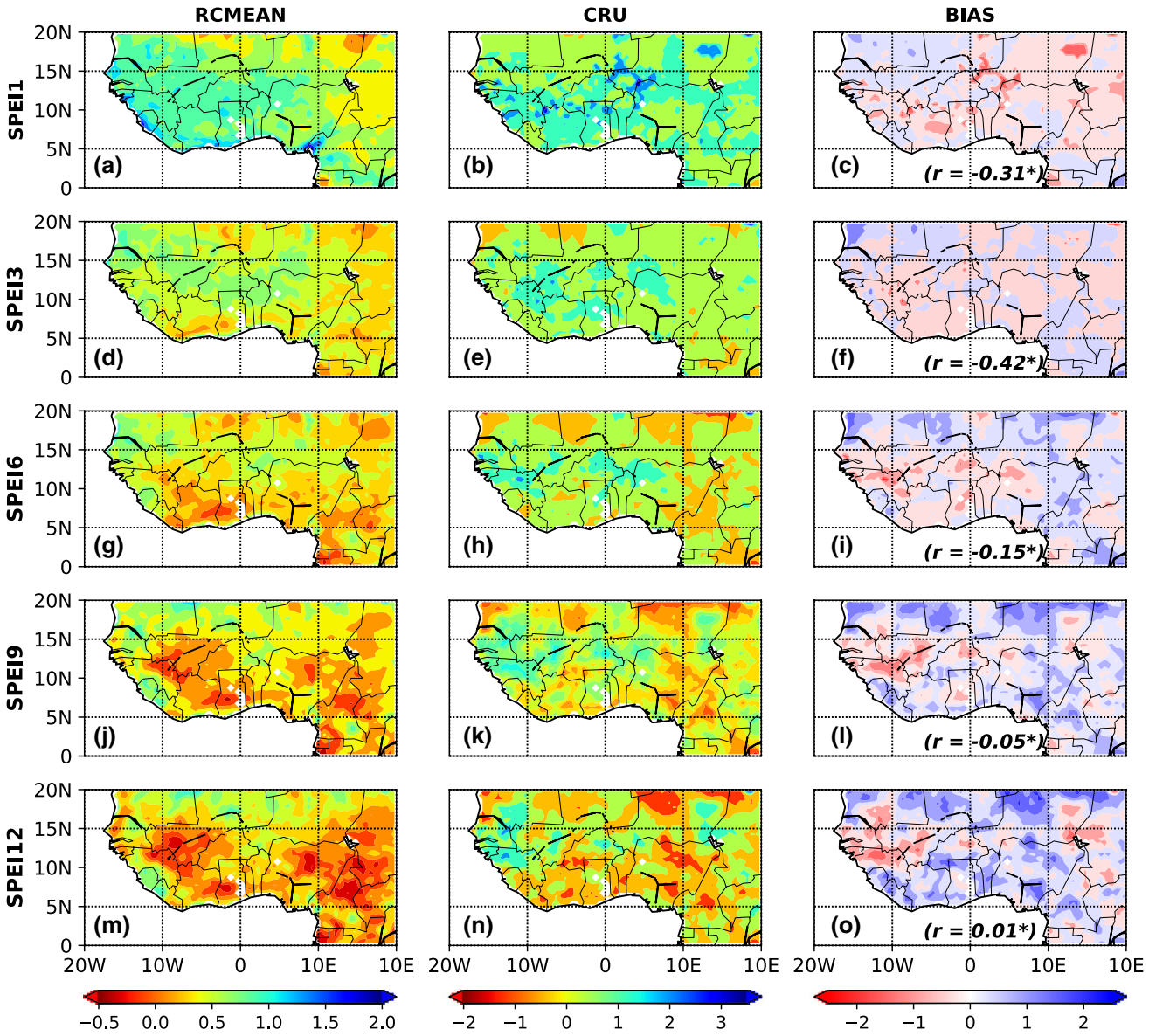

Fig. 4 Standardized Precipitation Evapotranspiration Index (SPEI) over West Africa for historical period for various drought types (SPEI1: meteorological drought, SPEI3 and SPEI6 : agricultural drought, SPEI9 and SPEI12: hydrological drought). RCMEAN is the ensemble mean of CORDEX-RCA4 models, CRU is the observed dataset, and BIAS = RCMEAN-CRU is the difference between the model ensemble mean and the observed; *r* is the correlation between the observed CRU and RCMEAN

ensemble mean of models. However, it has to be kept in mind that on a grid, the SPEI has either negative or positive values and its averaging could be the reason for the misrepresentation of both model ensemble mean and observed. It can also be mentioned based on Fig. 4 that the more the SPEI scale increases, the more the model improves its reproducibility with the observed pattern. Another factor can be the potential large discrepancy among the simulated patterns.

3.2 Assessment of the Extreme and Severe Dry Events for Historical Period

To explain the misrepresentation of ensemble mean SPEI pattern with respect to CRU (Fig. 4), the computation of the magnitude of drought frequency is undertaken. Figures 5 and 6 show, respectively, the frequency of extreme (SPEI < − 2) and severe (− 2 < SPEI < − 1.5) droughts in West Africa for the historical period for both the observed and the RCMEAN. The performance of the model in simulating drought intensity and frequency over the study area

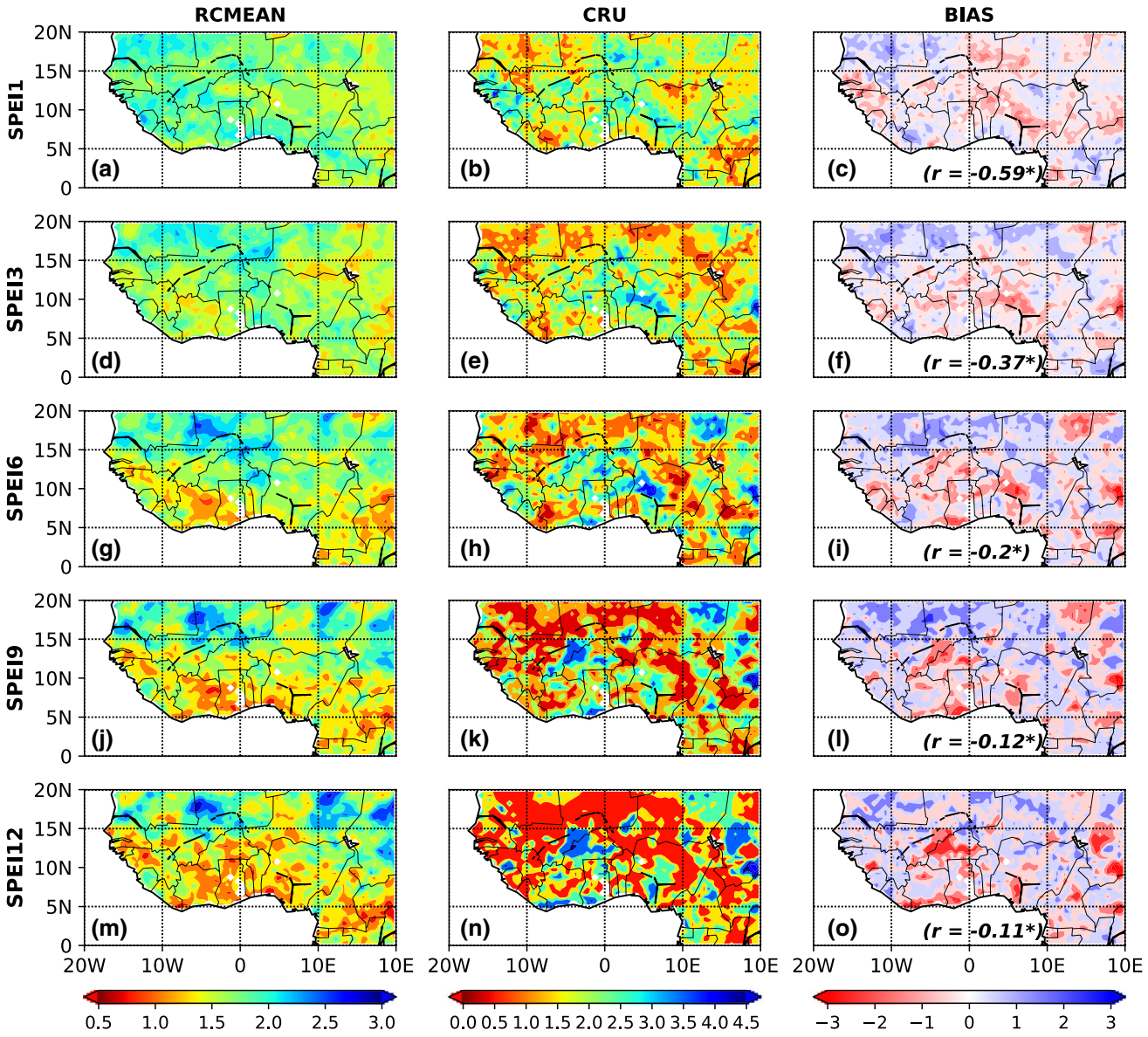

Fig. 5 Frequency of the extreme dry over West Africa for various drought types (SPEI1: meteorological drought, SPEI3 and SPEI6: agricultural drought, SPEI9 and SPEI12: hydrological drought). RCMEAN is the ensemble mean of CORDEX-RCA4 models, CRU is the observed dataset, and BIAS = RCMEAN-CRU is the difference between the model ensemble mean and the observed; *r* is the correlation between the observed CRU and RCMEAN

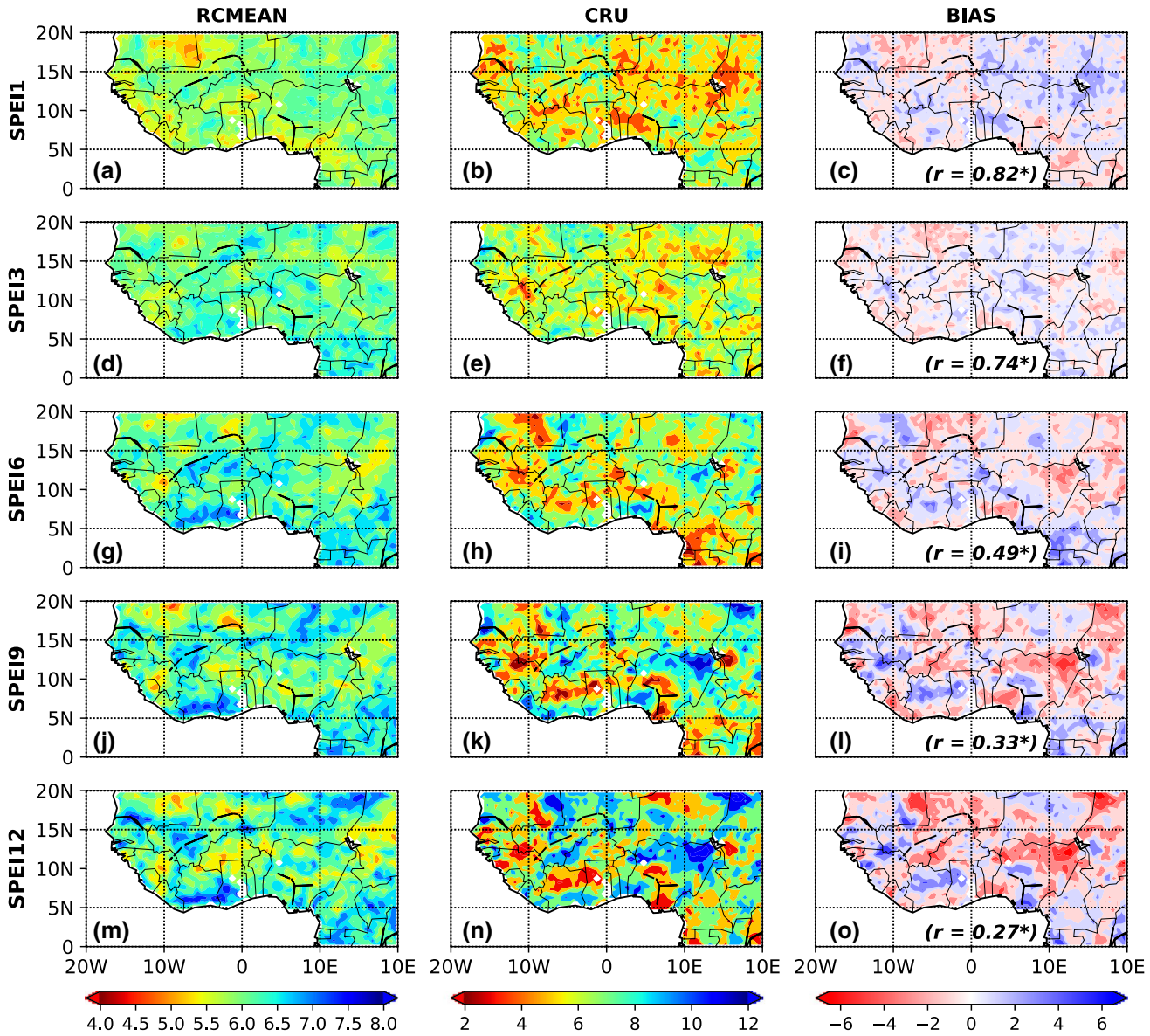

Fig. 6 Same as Fig. 5 but for severe dry events

depends on the scale of which the SPEI is computed. The model reproduces the extreme and severe droughts for each type of drought with positive correlation. The agreement of the model decreases when the scale of the SPEI increases (pointing out with the correlation *r* computed between the RCMEAN and CRU), which means that the RCMEAN captures the meteorological and agricultural extreme and severe droughts better than the hydrological extreme drought. However, the ensemble mean at the scale of meteorological and agricultural droughts overestimate the frequency of extreme drought events up to 2 events per decade at the northwestern part and the Gulf of Guinea. The underestimation of the frequency of extreme drought lies in the Gulf of Guinea for both agricultural and hydrological drought events. Nevertheless, the models do capture well the magnitude of hydrological extreme drought over Nigeria, Benin, south of Ghana, and northern part of Niger with a bias close to zero. According to the model, the high values of the frequency in extreme drought are located at the Gulf of Guinea, the Sahel, and the eastern part of the study area including Chad and the north of Nigeria for the agriculture drought. Conversely, the model records the low value of the frequency of agricultural extreme drought in Niger, Ghana, Cote d'Ivoire Guinea, and Cameroon. It shows that the frequency of severe drought is from 4 to 8 events per decade, while for the observed this frequency is between 2 and 12 events per decade. Globally at the scale of meteorological drought,

there is an overestimation of the frequency of severe drought except for countries as Mauritania, Mali, and Cameroon, which present an underestimation of 2 events per decade in response to the frequency to CRU. The model at the agricultural scale underestimates the severe drought over Chad, northern Nigeria, southern or Benin, Niger, and Mauritania up to 4 events per decade. The model fails to reproduce the hydrological severe drought; it widely underestimates the frequency of severe drought in Niger, Mali, Mauritania Nigeria, Chad, Benin, southern Ghana, and Cote d'Ivoire. The highest value for its misrepresentation is over northeastern Nigeria (a part of Lake Chad) and Mauritania, and northern of Chad where the model evaluates the magnitude of the hydrological severe drought about 7 events per decade against 12 events per decade according to the observation. The model for all types of severe drought overestimates the magnitude over Senegal, Mauritania, eastern of Mali, and the northern part of Niger, Cote d'Ivoire, and Ghana up to 4 events per decade.

3.3 Assessment of the Projection of Extreme and Severe Dry Events

Figures 7 and 8 present the variability of extreme and severe dry events, respectively, under different GWLs and various drought types. Figure 7 indicates that more than 80% of RCA4 models under the GWL1.5 °C show that West Africa experiences a northward increasing trend of extreme dry events (i.e., there is an increase in the frequency of extreme drought events compared to the historical period from the south to the northern part) which is materialized with the black cross (+). Conversely, for the GWL1.5 °C a southward decreasing trend of severe drought is recorded (proved with the horizontal black stripe in Fig. 8), and the frequency of the event increases from the meteorological drought to hydrological drought. In terms of frequency, over the Sahel,

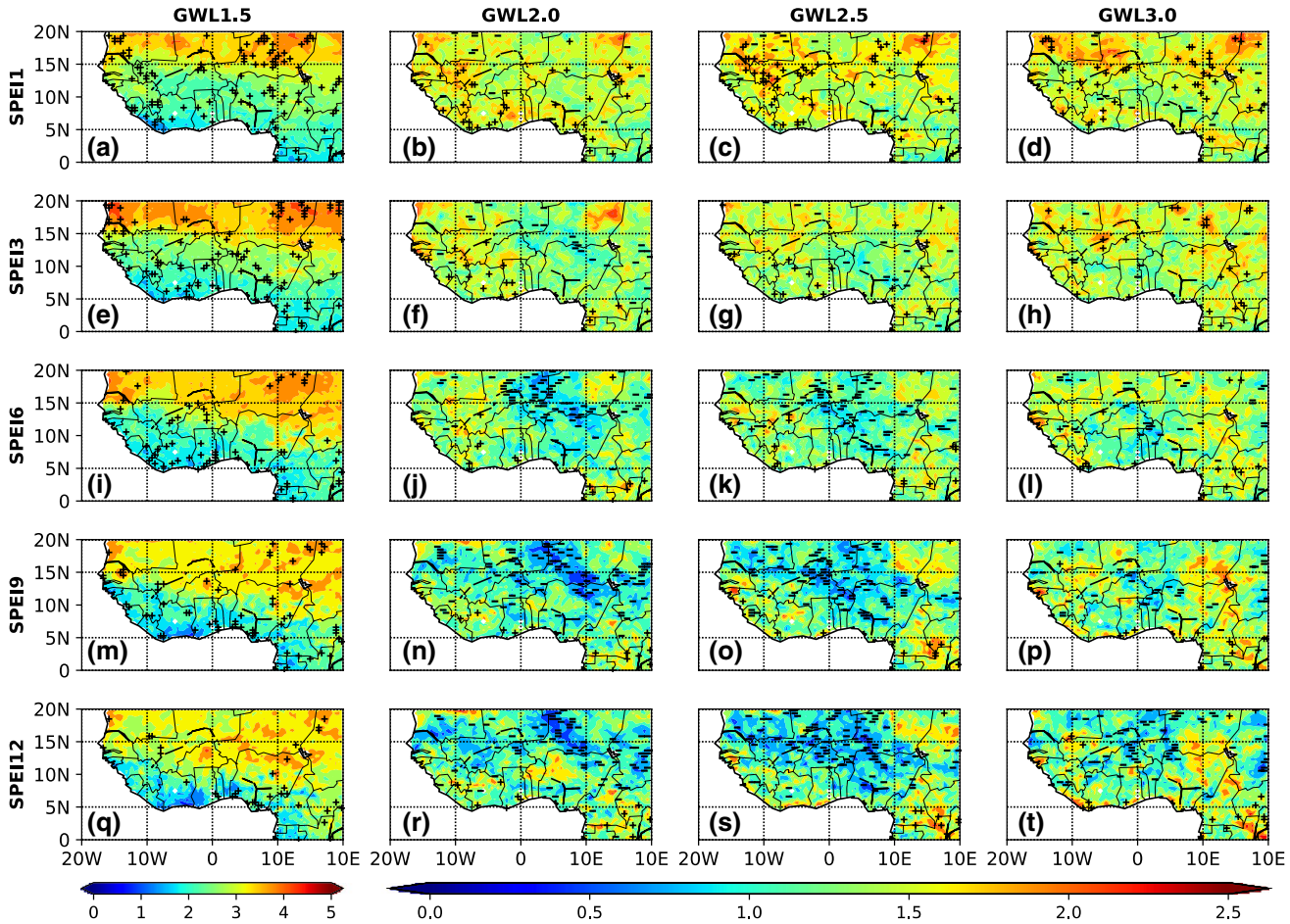

Fig. 7 Frequency of the extreme dry over West Africa for various drought types (SPEI1: meteorological drought, SPEI3 and SPEI6: agricultural drought, SPEI9 and SPEI12: hydrological drought) at different GWLs during the projection periods. The horizontal stripe (−) indicates that more than 80% of the models agree with a decreasing trend of extreme dry events, while the cross (+) shows that at least 80% of the models agree with an increasing trend of extreme dry events

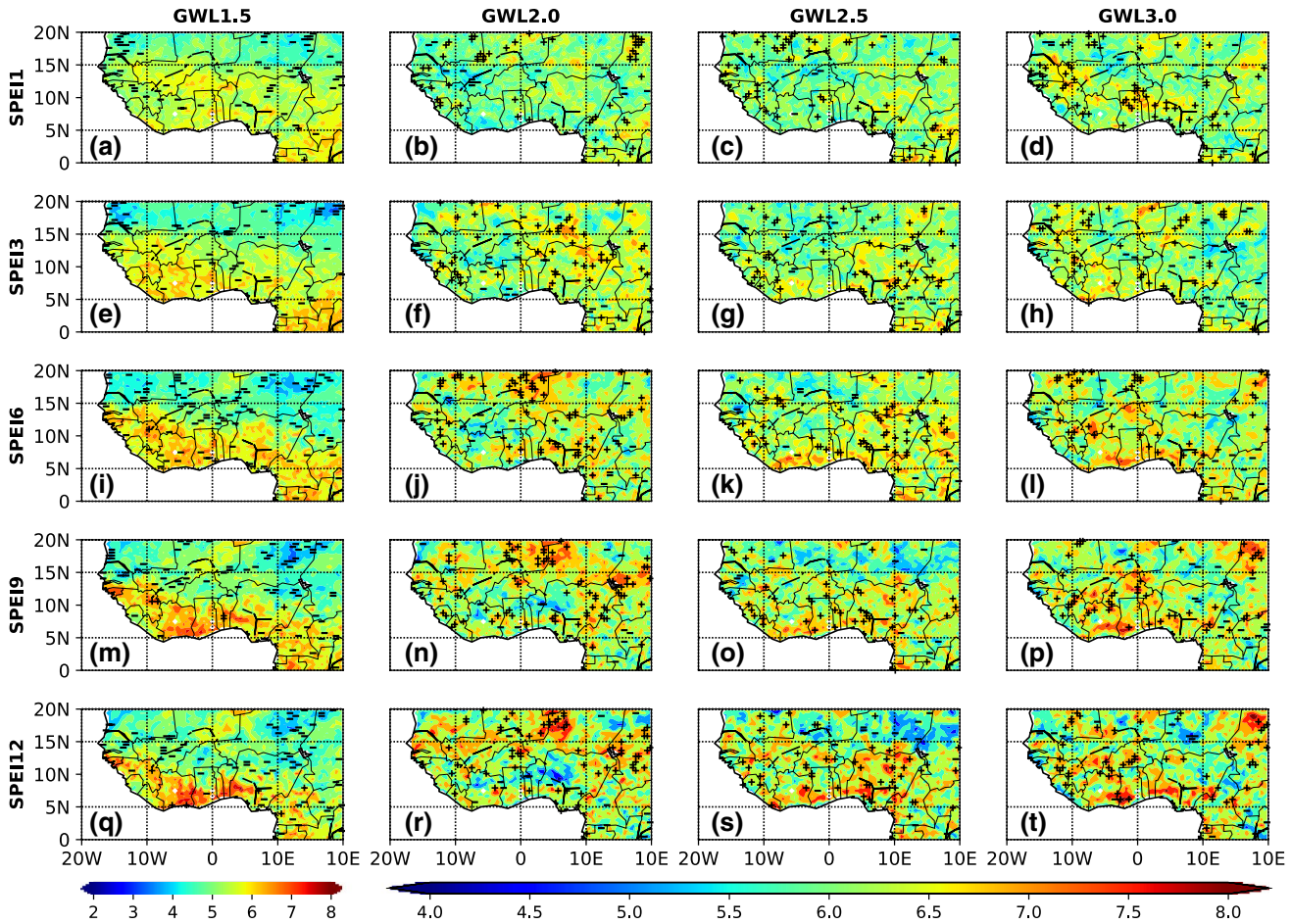

Fig. 8 Same as Fig. 7 but for severe dry events

the extreme dry weather frequency is above of 4 events per decade and about 3 events per decade in the Savanna. In the Gulf of Guinea, this frequency is about 2 events per decade. In the meteorological drought for the other GWLs (2.0 °C, 2.5, and 3.0 °C), the Gulf of Guinea and Savannah experienced an increase in extreme drought trends with a frequency of about 2 events per decade, while over Sahel and Savanna more than 80% of the models show a downtrend of the extreme dry event for agricultural and hydrological droughts. This decrease extends also to the Gulf of Guinea for the SPEI9 under GWL2.5. Only some coastal countries such as Ghana, Cote d'Ivoire, and Cameroon experience an increase in the extreme dry events during the projected periods. Globally, the frequency of the extreme drought is between 1 and 2 events per decade for the GWLs 2.0 °C, 2.5 °C, and 3.0 °C. However, it is projected a uniform pattern of extreme drought events over West Africa according to the RCA4 models.

In summary, under the interested GWLs used in this study, much variability has been noticed with the reference period. The ensemble mean of models shows either important extreme or severe dry events. Globally, under the GWL1.5 for all drought types studied, a recurrent increase in extreme dry events is noticed, particularly the Gulf of Guinea and Savanna for both events experienced an increasing trend, while the Sahel illustrates an increase in only extreme dry events. For the GWL 2.0, 2.5, and 3.0, at agricultural and hydrological drought scales, a high important decrease in the extremely dry events is perceived over the Savanna and the Sahel particularly around countries as Niger, Mali, Burkina Faso, Benin, and Nigeria. The coastal countries detect an increase in extremely dry events, while the southeastern area notes an increase in the extremely dry events. To figure out the causes of these various drought events recorded, an analysis on the concentration of the precipitation according to the simulations of CORDEX-RCA4 is undertaken.

3.4 Annual Variability of the Precipitation Concentration Index

The annual scale of the PCI calculated in this study varies generally across the study area from values greater or equal

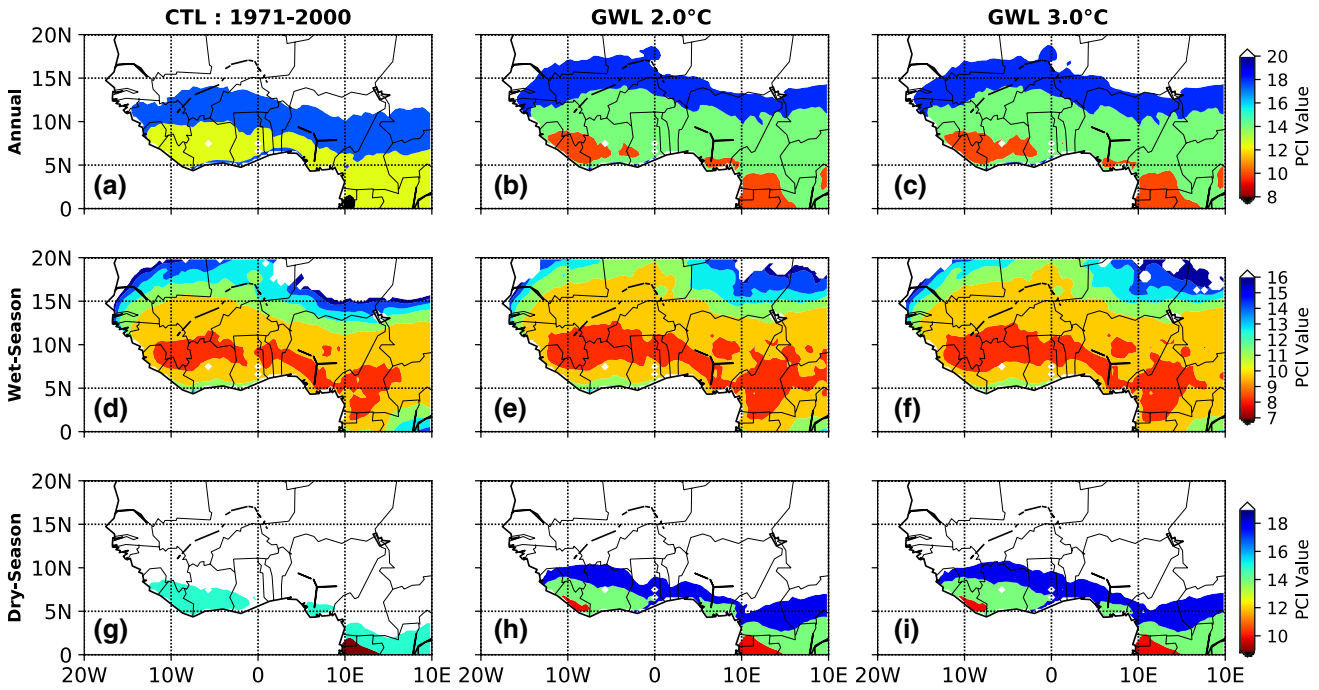

Fig. 9 Variability of PCI at annual and seasonal scales for the historical period (CTL: 1971–2000) and for projections of GWLs 2.0 °C and 3.0 °C

to 10, to higher than 20; according to Oliver's (1980) classification, this denotes a seasonal rainfall regime. Figure 9 presents the variability of PCI on annual, rainy season (wet season), and dry season periods over West Africa for the GWLs 2.0 °C and 3.0 °C. The display of PCI of GWLs 1.5 °C and 2.5 °C (not shown) is similar to the analysis of GWLs 2.0 °C and 3.0 °C. From Fig. 9a–c, the lower values recorded during the historical period (here called the control period or CTL) are between 10 and 13 on the Gulf of Guinea, thus illustrating a moderate precipitation concentration over this area. The seasonality is more pronounced in the transition area (the Savanna) with a PCI between 17 and 18, which shows how the precipitation concentration is irregularly distributed; lastly, the Sahel area has a high precipitation concentration (PCI>20), which means that the precipitation is strongly and irregularly distributed.

For the different GWLs studied, it is noticed that, for the Gulf of Guinea and the Savanna, an irregular precipitation concentration exists, except for some countries (Liberia and Côte d'Ivoire), which have a low precipitation concentration, while a strong irregular precipitation distribution is observed in the Sahel.

3.5 Seasonal Variability of the Precipitation Concentration Index

The PCI calculated for the seasonal scale shows complex spatial patterns of precipitation distribution in the area of study. Thus, Fig. 9d–f illustrates the uniform precipitation concentration (i.e., PCI values below 10, Oliver 1980) across the Gulf of Guinea and the Savanna. For the specified GWLs, the average of the uniform precipitation distribution extends toward the Sahel. The northern part of the study area records an irregular precipitation concentration ($16 \leq PCI \leq 20$) during the wet season.

Figure 9 (g–i: PCI for the dry season) shows that, during this period of the year selected, an irregular precipitation concentration is only observed over the Gulf of Guinea. All the other areas, such as the Savanna and the Sahel, have a strong irregular precipitation concentration, which means that the total precipitation occurs within 1 or 2 months.

The results from Fig. 9 (concerning the annual and seasonal evaluation) confirm that the precipitation in West Africa is uniformly distributed during rainy season in the Gulf of Guinea and the Savanna. Despite the global warming effect for all levels, this precipitation concentration does not change; on the contrary, it extends toward the Sahel. In general, the highest values of PCI are recorded over the Sahel, whereas the lowest occur over the Gulf of Guinea.

3.6 Variability of the Precipitation Concentration Degree and the Precipitation Concentration Period

Figure 10 displays the PCP and PCD. Figure 10a–c illustrates that the range of PCPs across West African region

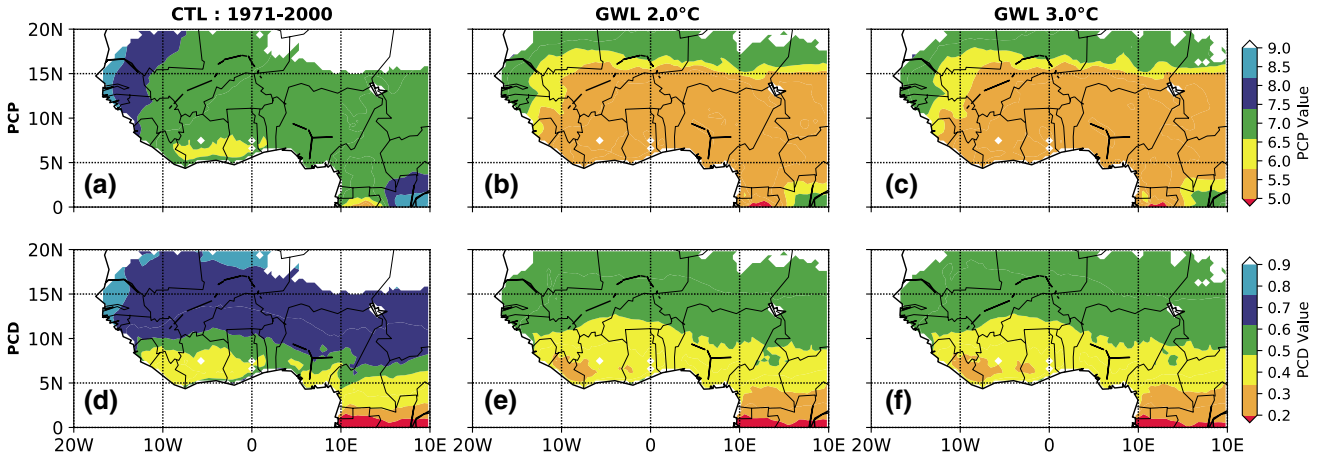

Fig. 10 Spatial distribution of yearly mean PCD and PCP for the historical period (CTL: 1971–2000) and at projections of GWLs 2.0 °C and 3.0 °C

for the present or future study periods is around 7 ± 2. This means that the yearly mean PCP on West Africa is from June to September, a period of rainfall production governed by the West African Monsoon (WAM). The highest value for the historical period (1971–2000, also referred to as the control period) is recorded over the northwestern part of West Africa, while for the projections, this value is located over the Sahel. The result confirms that the rainy season arrives earlier in the southern areas, followed by the transition area (the Savanna), before reaching the Sahel. The mean yearly PCDs (Fig. 10d–f) vary from 0.17 to 0.90, denoting the high variability of the precipitation concentration over West Africa. During the present period (Fig. 10d), the PCD values increase, suggesting the existence of a gradient across the Gulf of Guinea and Sahel. The lower values (0.17–0.60) are recorded over the Gulf of Guinea and the highest (> 0.80) in the Sahel. This gradient explains that precipitation is concentrated in fewer months over the Sahel than over the coastal areas. The same gradient dynamics is observed in the case of future projections, although the PCD values are reduced, compared to the historical period. The lower values here are between 0.17 and 0.50, and the higher values are between 0.5 and 0.6. For the future period, the precipitation concentration decreases, and the Savanna and Sahel have the same precipitation distribution. Furthermore, the GWLs indicate that the rainy season will start earlier than in the present (historical period). The highest concentration period for the Gulf of Guinea and the Savanna will be from May to July, while the concentration over the Sahel will be highest in August.

3.7 Daily Variability of Precipitation

Figure 11 presents the variations between the projection of each GWL and the present period. Higher values of CDD are observed in the northern part of the study area, while higher CWD values occur in the coastal areas. Comparing the patterns of Figs. 11a–d, i–l, it can be seen that the CDD decreases about 10 ± 5 days over the northeastern part of the study domain, both annually and during the rainy season. In the northern part, a significant variability of dry days occurs within the rainy season (for instance, a reduction over the northeastern area and an increase over the northwestern area), which means that the northeastern of the study domain is wetter under GWLs and the northwestern area is drier. The Gulf of Guinea has a very slight variability in respect of CDD for all GWLs studied, at both annual and rainy season scales. The projections of the GWLs 1.5 °C, 2.0 °C, 2.5 °C show essentially the same variability in the annual CDD, while the GWL 3.0 °C (Fig. 11i) shows a significant increase in the annual CDD. The CDD is projected to increase for 4–5 days over the Gulf of Guinea; in Mauritania and Senegal, the increase is projected to be 10 ± 2 days. Niger and Chad (which are characterized by a dry northeasterly flow crossing the Sahara desert) are projected to record a reduction of CDD with a range of 12 ± 2 days. This agrees with the results of Klutse et al. (2018), who illustrated a decrease for GWLs 1.5 °C and 2.0 °C, in terms of the number of CDD in West Africa during the rainy season, and the results of Sultan and Gaetani (2016), who reported a reduction in the number of dry days over central Africa.

In general, the CWD does not appear to record as many variations as was the case with the CDD. It varies slightly with 0 ± 3 days. Nonetheless, high and important variations can be noticed at several specific points. Figure 11e–h shows that CWD is projected to decrease by 10 ± 2 over the southern parts of Benin and Nigeria. A small increase in CWD of up to 2 days is also likely to be recorded over the Sahel.

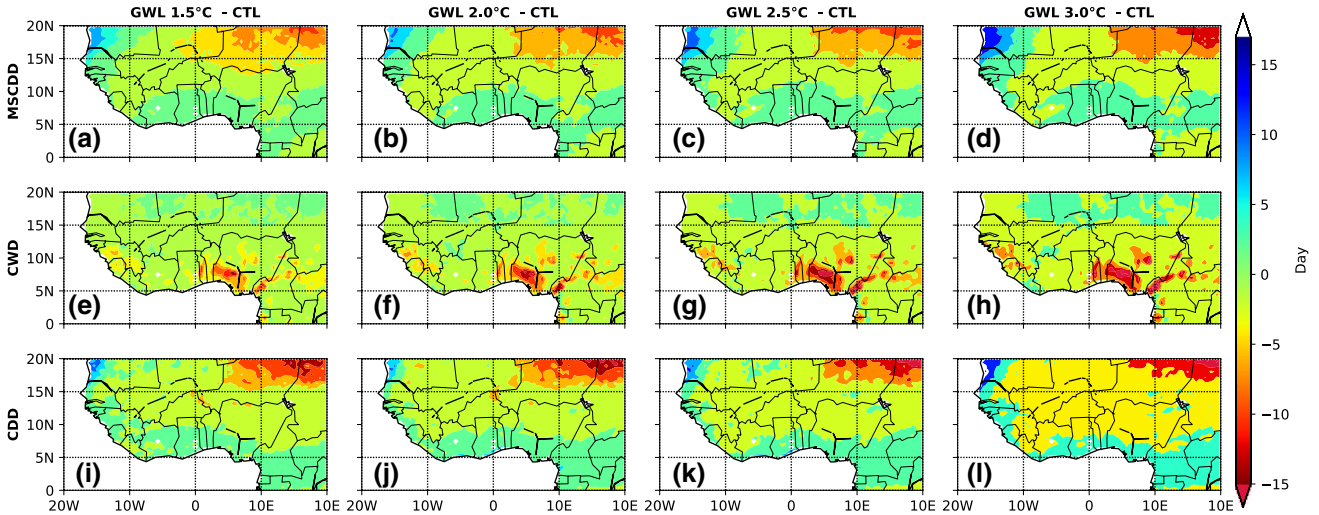

Fig. 11 Spatial distribution of the change in CDD during the rainy season (MSCDD), as well as the annual consecutive dry days (CDD) and the consecutive wet days (CWD)

4 Summary and Conclusion

West Africa is known to be particularly vulnerable to climate change due to high climate variability, high reliance on rain-fed agriculture, and limited economic and institutional capacity to respond to climate variability and change. In this context, better knowledge of how climate will change in West Africa, and how such changes will impact extreme climate events such as drought constituted the purposes of this study. The spatial distribution of SPEI values examined showed that during the historical period the Sahel and Savanna experimented extreme and severe droughts, specifically during years 1971–1974, 1977–1980, 1987–1989, 1994 and 1995, confirming the results from Masih et al. (2014), where it explained that droughts which occurred in Sahel and Savanna in 1972–1973, 1983–1984, and 1991–1992 were most intense and widespread. The results are also in agreement with the investigation on drought in West Africa by Hulme et al. (2001), Nicholson (2005), Van De Giesen et al. (2010), Kasei et al. (2010), Oguntunde et al. (2017a, b), and Diasso and Abiodun (2015). Under the RCP8.5 scenario, the Gulf of Guinea could be the wettest area, especially the coastal countries that signed with negative values of SPEI. A reduction of the driest episodes under GWLs was also found, particularly in the areas covering latitude 12ºN–16ºN, while an increase in extreme droughts for the coastal part of Liberia and Cameroon, Mali, Burkina Faso, Niger, Ivory Coast, Benin, Nigeria, and Chad is noticed. The relevant uncertainty shown in Figs. 2, 4, 5, and 6 of the model in response to the observed may be due to the bias in both GCMs and RCMs simulations (Abiodun et al. 2018). More focusing on the reduction of this bias may enhance the application of the results. In this study, to mitigate the effect of this bias for the applicability of the results, other indices such as PCI, PCP, and PCD were involved to explore the spatial distribution of precipitation, in order to reinforce the analyses from the SPEI's variabilities. The findings obtained with regard to the PCI illustrated that the main rainfall activity period over West Africa was between May and September. During the historical period, rainfall was uniformly well distributed over the Gulf of Guinea and the Savanna, while in the Sahel a more moderate and irregular precipitation concentration was recorded. Under all the GWLs (i.e., 1.5 °C, 2.0 °C, 2.5 °C and 3.0 °C), the moderate and irregular precipitation concentration was projected to reduce making appear more uniform distribution, except over the northeastern areas (Niger and Chad), which became the least dry according to all four GWLs. To obtain further detail about the period of the concentration of rainfall in West Africa, the PCP variable was calculated. It showed that the precipitation concentration increased gradually from the Gulf of Guinea to the Sahel, thus showing the existence of a south–north gradient. During the historical period (1971–2000), the highest rainfall concentration occurred in July–August over the Gulf of Guinea and the Savanna, while it was highest during September over the Sahel. The rainfall was found to be more concentrated in June–July over the Gulf of Guinea and the Savanna, and during August for the Sahel. In general, the degree of the concentration seemed to be more important in the Savanna–Sahel (with high values of PCD), due to the WAM system, which is led by the back-and-forth movement of the ITD between south and north.

Acknowledgements This work was funded by the German Federal Ministry of Education and Research (BMBF) through the West African Science Service Center on Climate Change and Adapted Land

Use (WASCAL) for providing to Gandome Mayeul L.D. Quenum the research fund.

Compliance with ethical standards

Conflict of interest The authors declare that they have no conflict of interest.

References

Abatzoglou JT, Rupp DE, Mote PW (2014) Seasonal climate variability and change in the pacific northwest of the united states. J Clim 27(5):2125–2142. https://doi.org/10.1175/JCLI-D-13-00218.1

Abiodun BJ, Makhanya N, Petja B, Abatan AA, Oguntunde PG (2018) Future projection of droughts over major river basins in Southern Africa at specific global warming levels. Theoret Appl Climatol. https://doi.org/10.1007/s00704-018-2693-0

Abramowitz M, Stegun IA (1964) Handbook of mathematical functions: with formulas, graphs, and mathematical tables (ninth Dove, Vol. 55). Dover, New York

Chou C, Lan C-W (2011) Changes in the annual range of precipitation under global warming. J Clim 1:222–235. https://doi.org/10.1175/JCLI-D-11-00097.1

Dai A, Trenberth KE, Qian T (2004) A global dataset of Palmer Drought Severity Index for 1870–2002: relationship with soil moisture and effects of surface warming. J Hydrometeorol 5:1117–1130

De Luis M, González-Hidalgo JC, Brunetti M, Longares LA (2011) Precipitation concentration changes in Spain 1946-2005. Nat Hazards Earth Syst Sci 11(5):1259–1265. https://doi.org/10.5194/nhess-11-1259-2011

Déqué M, Calmanti S, Bøssing O, Dell A, Fox C, Haensler A, Nikulin G, Teichmann C (2017) A multi-model climate response over tropical Africa at + 2 °C. Clim Serv 7:87–95. https://doi.org/10.1016/j.cliser.2016.06.002

Descroix L, Genthon P, Amogu O, Rajot JL, Sighomnou D, Vauclin M (2012) Change in Sahelian Rivers hydrograph: the case of recent red floods of the Niger River in the Niamey region. Global Planet Change 98–99:18–30. https://doi.org/10.1016/j.gloplacha.2012.07.009

Diasso U, Abiodun BJ (2015) Drought modes in West Africa and how well CORDEX RCMs simulate them. Theoret Appl Climatol 128(1–2):223–240. https://doi.org/10.1007/s00704-015-1705-6

Easterling DR, Meehl GA, Parmesan C, Changnon SA, Karl TR, Mearns LO (2000) Climate extremes: observations, modeling, and impacts. Science 289:2068–2075

Ebi KL, Bowen K (2016) Extreme events as sources of health vulnerability: drought as an example. Weather Clim Extremes 11:95–102. https://doi.org/10.1016/j.wace.2015.10.001

Egbebiyi TS (2016) Future Changes in Extreme Rainfall Events and African Easterly Waves over West Africa. University of Cape Town

Ezenwaji EE, Nzoiwu CP, Chima GN (2017) Analysis of precipitation concentration index (PCI) for Awka Urban Area. Hydrol Current Res 8(4):4–9. https://doi.org/10.4172/2157-7587.1000287

Fiala T, Ouarda TBMJ, Hladný J (2010) Evolution of low flows in the Czech Republic. J Hydrol 393(3–4):206–218. https://doi.org/10.1016/j.jhydrol.2010.08.018

Gao Y, Zhu X, Yu G, He N, Wang Q, Tian J (2014) Agricultural and Forest Meteorology Water use efficiency threshold for terrestrial ecosystem carbon sequestration in China under afforestation. Agric For Meteorol 195–196:32–37. https://doi.org/10.1016/j.agrformet.2014.04.010

Garner G, Van Loon AF, Prudhomme C, Hannah DM (2015) Hydroclimatology of extreme river flows. Freshw Biol 60(12):2461–2476. https://doi.org/10.1111/fwb.12667

Harris I, Jones PD, Osborn TJ, Lister DH (2014) Updated high-resolution grids of monthly climatic observations—the CRU TS3.10 dataset. International Journal of Climatology. https://doi.org/10.1002/joc.3711

Hulme M, Doherty R, Ngara T, New M, Lister D (2001) African climate change. Clim Res 1900–2100(17):145–168. https://doi.org/10.1002/jbmr.347

IPCC (2012) Managing the risks of extreme events and disasters to advance climate change adaptation. A special report of working groups I and II of the intergovernmental panel on climate change [Field, C.B., V. Barros, T.F. Stocker, D. Qin, D.J. Dokken, K.L. Ebi, M.D]

IPCC (2014) Climate change 2014: synthesis report. contribution of working groups I, II and III to the fifth assessment report of the intergovernmental panel on climate change [Core Writing Team, R.K. Pachauri and L.A. Meyer (eds.)]. In IPCC. Geneva, Switzerland, p 151

Joetzjer E, Douville H, Delire C, Ciais P, Decharme B, Tyteca S (2013) Hydrologic benchmarking of meteorological drought indices at interannual to climate change timescales: a case study over the Amazon and Mississippi river basins. Hydrol Earth Syst Sci 17(12):4885–4895. https://doi.org/10.5194/hess-17-4885-2013

Kasei R, Diekkrüger B, Leemhuis C (2010) Drought frequency in the Volta Basin of West Africa. Sustain Sci 5(1):89–97. https://doi.org/10.1007/s11625-009-0101-5

Klutse NAB, Ajayi V, Gbobaniyi EO, Egbebiyi TS, Kouadio K, Nkrumah F, Quagraine KA, Olusegun C, Diasso U, Abiodun BJ, Lawal K, Nikulin G, Lennard C, Dosio A (2018) Potential impact of 1.5°C and 2°C global warming on consecutive dry and wet days over West Africa. Environ Res Lett 1:1. https://doi.org/10.1088/1748-9326/aab37b

Kumi N, Abiodun BJ (2018) Potential impacts of 1.5 °C and 2 °C global warming on rainfall onset, cessation and length of rainy season in West Africa. Environ Res Lett 13(5):12–13. https://doi.org/10.1088/1748-9326/aab89e

L'Hôte Y, Mahé G, Somé B, Triboulet J-P (2002) Analysis of a Sahelian annual rainfall index from 1896 to 2000; the drought continues. Hydrol Sci J 47(4):563–572. https://doi.org/10.1080/02626660209492960

Le Barbé L, Lebel T, Tapsoba D (2002) Rainfall variability in West Africa during the years 1950-90. J Clim 15(2):187–202. https://doi.org/10.1175/1520-0442(2002)015%3c0187:RVIWAD%3e2.0.CO;2

Lebel T, Ali A (2009) Recent trends in the Central and Western Sahel rainfall regime (1990-2007). J Hydrol 375(1–2):52–64. https://doi.org/10.1016/j.jhydrol.2008.11.030

Lebel T, Cappelaere B, Galle S, Hanan N, Kergoat L, Levis S, Vieux B, Seguis L (2009) AMMA-CATCH studies in the Sahelian region of West-Africa: an overview. J Hydrol 375(1–2):3–13. https://doi.org/10.1016/j.jhydrol.2009.03.020

Li X, Jiang F, Li L, Wang G (2011) Spatial and temporal variability of precipitation concentration index, concentration degree and concentration period Xinjiang, China. Int J Climatol 31(11):1679–1693. https://doi.org/10.1002/joc.2181

Masih I, Maskey S, Mussá FEF, Trambauer P (2014) A review of droughts on the African continent: a geospatial and long-term perspective. Hydrol Earth Syst Sci. https://doi.org/10.5194/hess-18-3635-2014

Maúre G, Pinto I, Ndebele-Murisa M, Muthige M, Lennard C, Nikulin G, Nicholson SE (2018) The southern African climate under 1.5 °C and 2 °C of global warming as simulated by CORDEX regional climate models. Environ Res Lett 13(6):065002. https://doi.org/10.1088/1748-9326/aab190

Nicholson S (2005) On the question of the "recovery" of the rains in the West African Sahel. J Arid Environ 63(3):615–641. https://doi.org/10.1016/j.jaridenv.2005.03.004

Nikulin G, Jones C, Giorgi F, Asrar G, Büchner M, Cerezo-Mota R, Christensen OB, Déqué M, Fernandez J, Hänsler A, van Meijgaard E, Samuelsson P, Sylla MB, Sushama L, Sushama L (2012) Precipitation climatology in an ensemble of CORDEX-Africa regional climate simulations. J Clim 25(18):6057–6078. https://doi.org/10.1175/JCLI-D-11-00375.1

Nikulin G, Lennard C, Dosio A, Kjellström E, Chen Y, Hansler A, Kupiainen M, Laprise R, Mariotti L, Maule CF, van Meijgaard E, Panitz H-J, Scinocca JF, Somot S (2018) The effects of 1.5 and 2 degrees of global warming on Africa in the CORDEX ensemble. Environ Res Lett 13(6):1. https://doi.org/10.1088/1748-9326/aab1b1

Oguntunde PG, Abiodun BJ, Lischeid G (2017a) Impacts of climate change on hydro-meteorological drought over the Volta Basin, West Africa. Glob Planet Change 155(March):121–132. https://doi.org/10.1016/j.gloplacha.2017.07.003

Oguntunde PG, Lischeid G, Abiodun BJ (2017b) Impacts of climate variability and change on drought characteristics in the Niger River Basin. Stochast Environ Res Risk Assess, West Africa. https://doi.org/10.1007/s00477-017-1484-y

Oliver JE (1980) Monthly precipitation distribution: a comparative index. Prof Geogr 32(3):300–309. https://doi.org/10.1111/j.0033-0124.1980.00300.x

Palmer WC (1965) Meterological drought. Research Paper No. 45. US Department of Commerce. Weather Bureau, Washington, DC

Panthou G, Vischel T, Lebel T (2014) Recent trends in the regime of extreme rainfall in the Central Sahel. Int J Climatol 34(15):3998–4006. https://doi.org/10.1002/joc.3984

Paturel JE, Servat E, Delattre MO, Lubes-niel H (1998) Analyse de séries pluviométriques de longue durée en Afrique de l'Ouest et Centrale non sahélienne dans un contexte de variabilité climatique. Hydrol Sci J 43(6):937–946. https://doi.org/10.1080/02626669809492188

Petrow T, Merz B (2009) Trends in flood magnitude, frequency and seasonality in Germany in the period 1951-2002. J Hydrol 371(1–4):129–141. https://doi.org/10.1016/j.jhydrol.2009.03.024

Shi P, Wu M, Qu S, Jiang P, Qiao X, Chen X, Zhou M, Zhang Z (2015) Spatial distribution and temporal trends in precipitation concentration indices for the Southwest China. Water Resour Manag 29(11):3941–3955. https://doi.org/10.1007/s11269-015-1038-3

Sultan B, Gaetani M (2016) Agriculture in West Africa in the twenty-first century: climate change and impacts scenarios, and potential for adaptation. Front Plant Sci 7(August):1–20. https://doi.org/10.3389/fpls.2016.01262

Sung JH, Chung ES (2014) Development of streamflow drought severity–duration–frequency curves using the threshold level method. Hydrol Earth Syst Sci 18(9):3341–3351. https://doi.org/10.5194/hess-18-3341-2014

Teuling AJ, Van Loon AF, Seneviratne SI, Lehner I, Aubinet M, Heinesch B, Prasse H, Spank U (2013) Evapotranspiration amplifies European summer drought. Geophys Res Lett 40(10):2071–2075. https://doi.org/10.1002/grl.50495

Trambauer P, Dutra E, Maskey S, Werner M, Pappenberger F, Van Beek LPH, Uhlenbrook S (2014) Comparison of different evaporation estimates over the African continent. Hydrol Earth Syst Sci 18(1):193–212. https://doi.org/10.5194/hess-18-193-2014

Van De Giesen N, Liebe J, Jung G (2010) Adapting to climate change in the Volta Basin, West Africa. Curr Sci 98(8):1033–1037

Vicente-Serrano SM, Beguería S, López-Moreno JI (2010) A multiscalar drought index sensitive to global warming: the standardized precipitation evapotranspiration index. J Clim 23(7):1696–1718. https://doi.org/10.1175/2009JCLI2909.1

Vicente-Serrano SM, Beguería S, Lorenzo-Lacruz J, Camarero JJ, López-Moreno JI, Azorin-Molina C, Revuelto J, Morán-Tejeda E, Sanchez-Lorenzo A (2012) Performance of drought indices for ecological, agricultural, and hydrological applications. Earth Interact. https://doi.org/10.1175/2012EI000434.1

Wang X, Zhang J, Yang Z (2013) Historic water consumptions and future management strategies for Haihe River basin of Northern China. Mitig Adapt Strateg Glob Change. https://doi.org/10.1007/s11027-013-9496-5

Zargar A, Sadiq R, Naser B, Khan FI (2011) A review of drought indices. Environ Rev 19:333–349. https://doi.org/10.1139/A11-013

Zhai J, Su B, Krysanova V, Vetter T, Gao C, Jiang T (2010) Spatial variation and trends in PDSI and SPI indices and their relation to streamflow in 10 large regions of china. J Clim 23(3):649–663. https://doi.org/10.1175/2009JCLI2968.1

Zhang LJ, Qian YF (2003) Annual distribution features of the yearly precipitation in China and their interannual variations. Acta Metall Sin 17:146–163

Zhang Q, Liu CX, Gemmer M, Chen YD, Liu C (2009) Changing properties of precipitation concentration in the Pearl River basin, China. Stoch Env Res Risk Assess 23:377–385. https://doi.org/10.1007/s00477-008-0225-7